Heliyon 9 (2023) e18508

Contents lists available at ScienceDirect

Heliyon

journal homepage: www.cell.com/heliyon

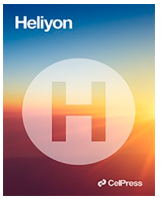

Assessing coastal vulnerability and land use to sea level rise in Jeddah province, Kingdom of Saudi Arabia

Abdulrazak H. Almaliki [a], Bilel Zerouali [b], Celso Augusto Guimarães Santos [c], Abdulrhman A. Almaliki [d], Richarde Marques da Silva [e,*], Sherif S.M. Ghoneim [f], Enas Ali [g]

[a] Department of Civil Engineering, College of Engineering, Taif University, P.O. BOX 11099, Taif 21944, Saudi Arabia
[b] Vegetal Chemistry-Water-Energy Laboratory, Department of Hydraulic, Faculty of Civil Engineering and Architecture, Hassiba Benbouali, University of Chlef, B.P. 78C, Ouled Fares, 02180, Chlef, Algeria
[c] Department of Civil and Environmental Engineering, Federal University of Paraíba, 58051-900 João Pessoa, Paraíba, Brazil
[d] Department of Computer Science, Swansea University, Swansea, Wales, UK
[e] Department of Geoscience, Federal University of Paraíba, 58051-900 João Pessoa, Paraíba, Brazil
[f] Department of Electrical Engineering, College of Engineering, Taif University, P.O. BOX 11099, Taif 21944, Saudi Arabia
[g] Faculty of Engineering and Technology, Future University in Egypt, New Cairo 11835, Egypt

ARTICLE INFO

Keywords:
Flooding modeling
Natural hazards
Sea level predicted
Eight-side rule
Inundated
Infrastructures
Decision-makers
Sustainable development

ABSTRACT

Sea level rise is one of the most serious outcomes of increasing temperatures, leading to coastal flooding, beach erosion, freshwater contamination, loss of coastal habitats, increased soil salinity, and risk of damage to coastal infrastructures. This study estimates the vulnerability to inundation for 2100 in coastal zones in Jeddah Province, Kingdom of Saudi Arabia, under various sea level rise (SLR) scenarios of 1, 2, 5, and 10 m. The predicted flooding was estimated using a combination of factors, including SLR, the bathtub model, digital elevation model, climate scenarios, and land use and land cover. The climate scenarios used were Representative Concentration Pathway (RCP) scenarios 1.9, 2.6, 4.5, and 8.5. The results of the SLR scenarios of 1, 2, 5, and 10 m revealed that 1.6, 4.7, 14.9, and 30.6% (or 88, 214, 679, 1398 km^2) of the study area's coast could be classified as inundated areas. The various SLR scenarios can inundate 3.3 to 34% of the road area/length. The inundated built-up and road areas were estimated to range between 0.31 and 0.79 km^2, accounting respectively for 1.18 to 3.01% of the total class areas for 1-meter and 2-meter SLR scenarios. In contrast, the inundated area will be significant in the situation of 5 and 10 m SLR scenarios. Regarding the case of a 10-meter SLR scenario, the inundation will negatively impact the built-up and road infrastructure areas, inundating 8.9 km^2, with industrial infrastructures affected by inundation estimated at 0.21 km^2, followed by green space infrastructures at 0.013 km^2. The spatial information based on various SLR scenario impact mapping for Jeddah Province can be highly valuable for decision-makers to better plan future civil engineering structures within the framework of sustainable development.

* Corresponding author.
E-mail addresses: a.almaliki@tu.edu.sa (A.H. Almaliki), bilel.zerouali@yahoo.fr (B. Zerouali), celso@ct.ufpb.br (C.A.G. Santos), 2203911@swansea.ac.uk (A.A. Almaliki), richarde@geociencias.ufpb.br (R.M. Silva), S.ghoneim@tu.edu.sa (S.S.M. Ghoneim), enas.ali@fue.edu.eg (E. Ali).

https://doi.org/10.1016/j.heliyon.2023.e18508
Received 30 April 2023; Received in revised form 26 June 2023; Accepted 19 July 2023
Available online 23 July 2023

1. Introduction

Climate change is a significant environmental phenomenon worldwide. It has the potential to negatively affect coastal areas, agricultural production, water resources, livelihoods, forests, and global health and eventually create poverty and food insecurity [1–3]. In the short-term, climate change will impact global development, as it has the potential to slow down the world's ability to achieve sustainable development [4,5].

Two aspects of global warming contribute to increasing sea levels. The first is the melting of ice masses and frozen rivers, and the second involves the enlargement of seawater volume due to increased temperatures. Climate change-induced sea level rise (SLR) will increase stress on coastal systems, mainly those with low resilience potentials and adaptive capacities [6–8]. SLR will affect coastal regions in terms of land inundation and shoreline instability. Inundation problems associated with SLR will have adverse impacts on coastal systems such as protection structures, infrastructure, coastal groundwater aquifers, water resources, stormwater drainage systems, cultural and historic resources, and land salinization. The anticipated consequences of rising sea levels include disruption to ecosystems, diminished agricultural output, alterations in disease prevalence, financial setbacks, and the forced relocation of susceptible populations [9–11].

Currently, sea levels are on the rise and this trend is likely to persist for centuries, irrespective of any reductions in greenhouse gas (GHG) emissions and achieving stability in atmospheric concentrations. From 1901 to 2010, the global mean sea level increased at an average rate of 1.7 (1.5 to 1.9) mm annually. This rate accelerated to 2.0 (1.7 to 2.3) mm/year from 1971 to 2010, and further increased to to 3.2 (2.8 to 3.6) mm/year from 1993 to 2010 [12]. Furthermore, Ref. [13] assessed the average global sea level rise from 1993 to 2009 to be 3.2 ± 0.4 mm/year using satellite measurements and 2.8 ± 0.8 mm/year utilizing in-situ data. From 1880 to 2009, the global sea level increased by approximately 210 mm. The linear trend between 1900 and 2009 was 1.7 ± 0.2 mm/year, while it was 1.9 ± 0.4 mm/year from 1961 onwards. Ref. [14] employed data from 1900 to 2008 to establish the global mean sea level (GMSL), revealing a rising trend of 1.1 mm/year with notable inter-annual and decadal fluctuations. Ref. [15] corroborated this trend for the period from 1900 to 2005, as most modeled estimates aligned with the calculated rate of 1.7 mm/year. In Ref. [16], researchers reconstructed sea level rise since 1990 using separate observations and associated uncertainties. They concluded that the combined contributions to SLR from ocean thermal expansion, ice mass loss, and alterations in terrestrial water storage align with observed SLR trends and multi-decadal variability at both global and basin levels.

A variety of time series have been created by researchers across the globe to study eustatic sea-level fluctuations [17–19]. For instance, the Intergovernmental Panel on Climate Change (IPCC) estimated a global increase of 23 to 96 cm between 1990 and 2100, with an average value of 55 cm [20]. Furthermore, the Intergovernmental Panel on Climate Change (IPCC) in its fifth assessment report (AR5) [21] predicted an increase in global mean sea level rise ranging from 0.17 m to 0.82 m during the mid to late parts of the 21st century. The extent of this increase depends on the optimism or pessimism of the considered scenarios. The latest IPCC report [22] presented five distinct representative emissions scenarios to study how the climate might react to a broader range of GHG emissions, land use changes, and air pollutant futures than those considered in the IPCC's Fifth Assessment Report (AR5). These scenarios, which are based on changes in the climate system relative to the 1850–1900 period, are referred to as Shared Socio-economic Pathways (SSP) and supersede the earlier Representative Concentration Pathways (RCP) scenarios. They include SSP1-1.9, SSP1-2.6, SSP2-4.5, SSP3-7.0, and SSP5-8.5. This document predicts a 0.28–0.55 m rise in global sea level for the very low GHG emissions scenario (SSP1-1.9) and a 0.63–1.01 m increase for the very high GHG emissions scenario (SSP5-8.5).

Integration of remote sensing (RS) data with other geospatial datasets, such as climate models and socio-economic data, allows for comprehensive coastal vulnerability assessments [23–25]. RS techniques play a crucial role in assessing coastal vulnerability to SLR. By analyzing remotely sensed data, scientists can monitor changes in coastal areas over time, identify vulnerable areas, and assess the impacts of sea level rise [26,27]. Remote sensing methods like satellite altimetry, Light Detection and Ranging (LiDAR), and radar interferometry can measure seafloor depth and coastal topography [28]. These data help determine the shape and elevation of coastal areas, including low-lying regions prone to flooding or erosion. Furthermore, by comparing historical and current RS imagery, scientists can identify areas experiencing erosion, accretion, or landward migration due to SLR [29,30]. RS techniques help classify and map coastal land cover types, such as forests, wetlands, urban areas, and agricultural land [31–33]. This information aids in identifying vulnerable ecosystems and areas at risk of inundation [34]. In addition, interferometric synthetic aperture radar (InSAR), LiDAR, Satellite Altimetry, and Unmanned Aerial Vehicles (UAVs) help detect SLR, land subsidence, and erosion hotspots [35–38].

Within this framework, several studies on SLR in KSA and worldwide have been documented [39–45]. We can cite the study of Al-Mutairi et al. [46] that examines the vulnerability of Kuwait's coastal zone to SLR from environmental and economic perspectives. At the national scale, applying the Bruun rule reveals that the investigated beaches would be completely eroded with a 1-m increase in sea level. Moreover, SLR ranging from 0.5 to 2 m would result in the inundation of 1.4%–4.8% of Kuwait's coastal zone, forcing 0.28%–1% of residents to abandon their homes and leading to residential losses of $3,463 to $11,142 million. The transportation sector would also suffer damage to approximately 1.5%–5% of its road network under these scenarios. Furthermore, the impact of SLR extends to Kuwait Bay, causing damage to its ecosystems. The consequences of SLR vary across different areas due to factors such as natural barriers, shoreline type, coastal structures, and the type of urban development. The study of Ref. [47] focused on the potential impacts of SLR on Damietta Governorate, which is particularly vulnerable due to its low-lying sandy coast. To estimate shoreline retreat, the Bruun rule, Landsat ETM+7, and digital elevation model (DEM) are used. The results indicate that if SLR reaches 1 m, approximately 254 square kilometers (16% of the governorate's total area) will be inundated. In a scenario with a 2-m SLR, the submerged area would expand to 661 square kilometers, representing 64% of Damietta's area. However, the application of the Bruun rule suggests that SLR would have a minimal impact on coastline erosion. Furthermore, Ref. [48] assessed the impacts of coastal flooding in Port Said city, Egypt, in relation to SLR using GIS, LULC, and DEM databases. The study finds that under the anticipated SLR scenarios of 1.0, 2.0, and

3.0 m, the estimated inundation areas are 827.49, 1072.67, and 1179.41 square kilometers, respectively. These findings demonstrate that the expected coastal flooding scenarios would have significant impacts on the LULC classes and coastal features in the study area.

SLR has serious physical effects on coastal areas and cities, primarily in the form of flooding and inundation risks, as in the case of Jeddah Province in the Kingdom of Saudi Arabia (KSA). The Jeddah coastal zone was therefore investigated to assess its vulnerability to SLR-related effects. Previous studies focused on tidal dynamics and climate change's effects on marine life, fish production, temperature changes, or rainfall rates [49–57]. Saudi Vision 2030 aims to improve the living standards of Saudi citizens by expanding the economy and enhancing their quality of life. Moreover, Saudi Vision 2030 promotes and supports construction initiatives, making the protection of cities against SLR a critical step toward achieving this sustainable vision. Given the risks of flooding as a result of the increasing sea levels stemming from climate change, the present research aims to analyze the projected SLR in 2100 suggested by IPCC AR6 [22] on the Jeddah Province coastal zone. The study area was extended to the south and north to encompass the entire province of Jeddah, resulting in a total length of 170 km for the irregular coast studied.

2. Study area

Jeddah Province, one of the governorates in the Makkah Region, is on the western border of KSA adjacent to the Red Sea shoreline (Fig. 1). Positioned between 20°13′55″ N to 22°05′25″ N and 38°15′31″ E to 39°40′00″ E, it lies approximately 949 km from Riyadh, the political capital of KSA. Jeddah is the second-largest city in KSA after the capital city, Riyadh, and serves as the largest port on the Red Sea, establishing itself as a center for business and finance in KSA. As KSA's economic and tourism capital, Jeddah has a population of about 4,781,000 people [52]. The city's coastline extends for more than 48 km along the Red Sea.

Jeddah serves as the gateway to the two holiest mosques for Muslims, located in Makkah and Madina. These sites attract a large number of visitors each year. The topography of Jeddah is characterized by a mixture of coastal plains, hills, and valleys. The coastal areas feature sandy beaches and coral reefs along the Red Sea shoreline. Progressing inland, the terrain gradually transitions to rocky plateaus, wadis (dry riverbeds), and small mountain ranges, including the Hijaz Mountains to the east. The province's climate is classified as a hot desert, characterized by long, hot summers and mild winters. High temperatures persist throughout the year, often exceeding 40 °C in the summer, and even reaching up to 48 °C. Jeddah Province experiences minimal rainfall, most of which occurs during the winter months. However, despite the annual precipitation being only about 60 mm, heavy thunderstorms are common

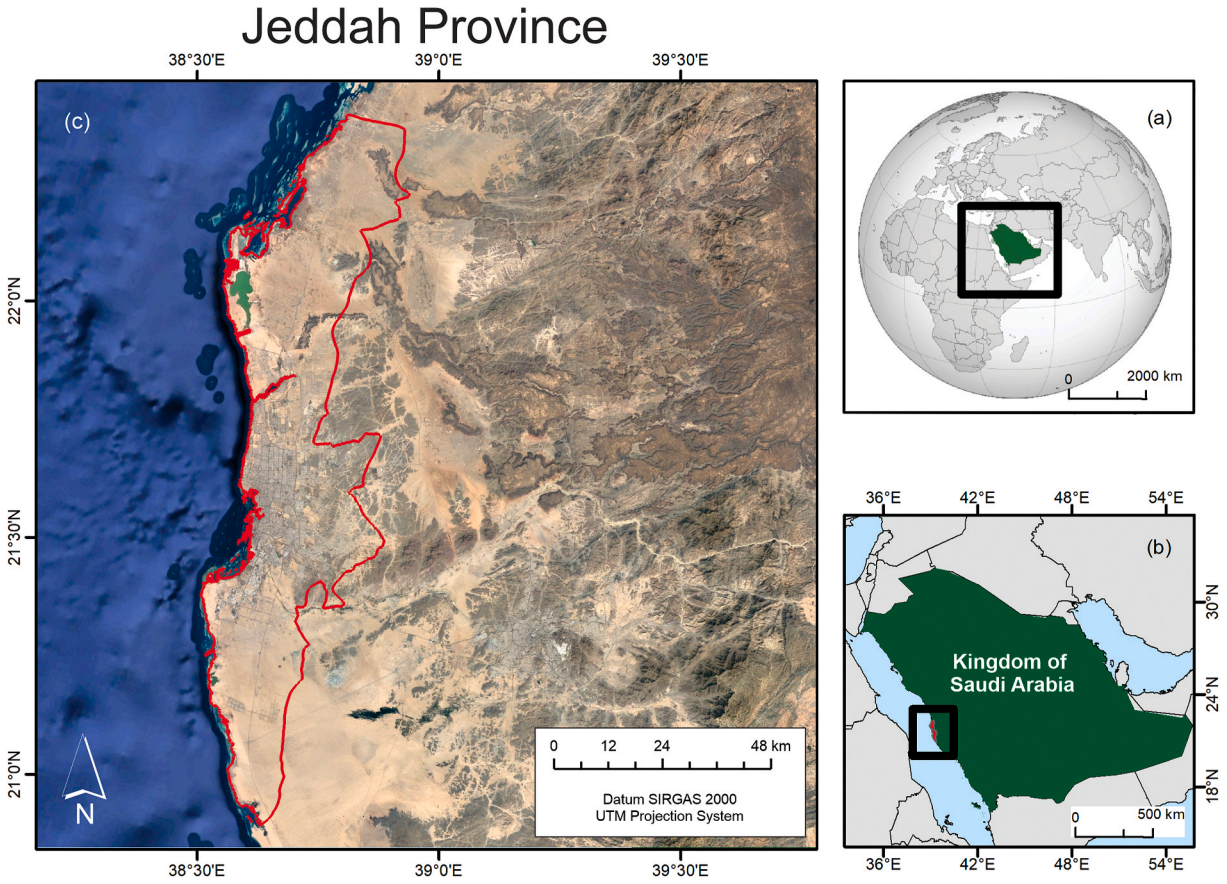

Fig. 1. Geographic map showing the location of Jeddah Province in relation to the overall elevation profile of Saudi Arabia.

during the winter [58].

3. Materials and methods

3.1. Tide gauge measurements

Hourly water levels were measured at Jeddah Port twelve times a day (every 2 h). Two time series datasets were collected; the first was recorded from January 2012 through April 2016, while the second spanned from February 2017, until July 2021 (Fig. 2 and Table 1). Each dataset was obtained from a specific location near Jeddah Port. The databases were sourced from the General Authority for Survey and Geospatial Information (GASGI) [59]. The geo-coordinates for both locations and the measuring information are shown in Table 1.

To estimate the SLR trend, the two datasets were treated as a single set, given that they were measured in the same environment, in close proximity, and by the same authority. The measured datasets were adjusted and analyzed, taking into account differences in altitude and omitting any outlier values. Fig. 2 illustrates the hourly data for the combined dataset. This dataset was analyzed to assess the annual SLR trend and can be used to study ocean currents, wave patterns, and other oceanographic phenomena. The tide levels, as measured by the gauge, are characterized by high temporal variability, and in many cases, they can reach 1 m (Fig. 2).

3.2. Sea level rise and inundation modeling

A flood assessment model, referred to as the zero-side rule approach (known as the bathtub approach), was utilized in this study. The bathtub approach is widely utilized for SLR inundation effects assessments due to its simplicity and applicability to large areas (Fig. 2). The bathtub model is very useful for understanding and predicting inundation, which occurs when an area is flooded with water. Inundation may be attributed to an array of elements, such as heavy precipitation, storm surge, and rising sea levels. By using the bathtub model, GIS can simulate how water moves through a hydrological system and accumulates in low-lying areas, allowing for predictions of where inundation is likely to occur [60,61]. Inundation modeling using the bathtub model and GIS typically involves creating a DEM of the area. The DEM is utilized to calculate changes in elevations and identify areas at risk of flooding [62–64]. Some GIS maps commonly used in the bathtub approach include (1) elevation maps: These maps display the elevation of the coastal area, including the shoreline, inland areas, and topographic features; (2) inundation maps: these maps depict the potential areas that could be affected by sea level rise and experience inundation; (3) vulnerability maps: these maps assess the vulnerability of the coastal area to sea level rise, taking into account factors such as elevation, coastal morphology, infrastructure, and ecological systems; (4) exposure maps: these maps illustrate the exposure of different elements in the coastal area to sea level rise. This includes infrastructure, critical assets, ecosystems, and population centers; (5) risk maps: these maps combine information on exposure, vulnerability, and potential impacts to provide a comprehensive understanding of the risk associated with sea level rise; (6) adaptation strategy maps: these maps illustrate the spatial distribution of proposed or implemented adaptation measures aimed at mitigating the risks of sea level rise; and (7) socioeconomic impact maps: these maps integrate demographic, economic, and social vulnerability data with sea level rise scenarios.

The no-elevation margin method stipulates that a grid cell is considered submerged when its elevation value falls below the estimated SLR, and even a slight deviation below this threshold classifies the grid cell as being underwater [65–67]. The four-side and eight-side rule methods take into account that a grid cell is only inundated if its elevation is beneath sea level and is connected to either an adjacent inundated grid cell or open water. The four-side rule applies if a grid cell is connected to an inundated cell in either cardinal or diagonal directions, whereas the eight-side rule applies if a grid cell is connected to an inundated cell in the cardinal directions. According to Ref. [65], the four-sided and eight-sided rules may underestimate and overestimate surface flow connections, respectively. The predicted flooding (F) at the grid cell is given by Equation (1):

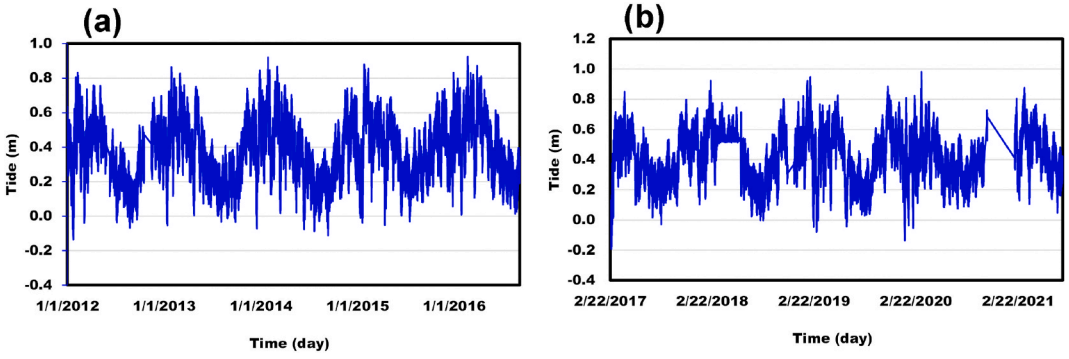

Fig. 2. Measured hourly tide gauge measurements at (a) old site and (b) new site in Jeddah.

Table 1
Tide gauge measurement information.

Location	Latitude	Longitude	Altitude (m)	Measuring period	
				From	To
Old Site	21°29′59.4″	39°09′46.4″	2.16	January 1, 2012	April 9, 2016
New Site	21°34′23.7″	39°06′32.6″	2.27	February 22, 2017	July 31, 2021

$$F_{x,y} = \begin{cases} E_{x,y} \leq S, 1 \\ C_i \\ E_{x,y} \leq S, 1 \end{cases} \quad (1)$$

where F is binomial, representing either not inundated (0) or inundated (1). E stands for the elevation at position x, y, S denotes the projected sea level, and C describes the connectivity, where not linked is 0 and linked is 1. Furthermore, i is an integer identifying the type of bathtub model used: zero-side rule, four-side rule, or eight-side rule. Fig. 3 provides a straightforward definition of inundated areas and demonstrates the connection between SLR and impacted land use zones.

To calculate the area in m^2 of each land use type potentially inundated by various levels of SLR, the number of pixels must first be converted into an area. This is achieved by multiplying the number of pixels by the width of the pixel in meters, and then by the height of the pixel in meters. As the height and width represent the resolution of the DEM, the following equation is used:

$$Area = Number\ of\ pixels \times height \times width \quad (2)$$

where the height and width of the pixel are both equal to 30 m.

Some studies have demonstrated that the bathtub approach and more complex approaches may be effective in specific circumstances [67,68]. The bathtub approach has been used to delineate coastal areas vulnerable to SLR by accurately identifying projected inundation areas [69,70]. In this context, some coastal areas may not project inundation due to dynamic responses driven by various factors. These dynamic responses can influence coastal processes and alter the extent or timing of inundation. Examples of these dynamic responses include coastal erosion and accretion, saltmarsh and wetland behavior, and the presence of coastal structures and natural barriers. As a result, the use of the bathtub model to project vulnerable areas in coastal regions does not necessarily imply that those areas will inevitably become part of the open sea, devoid of any land.

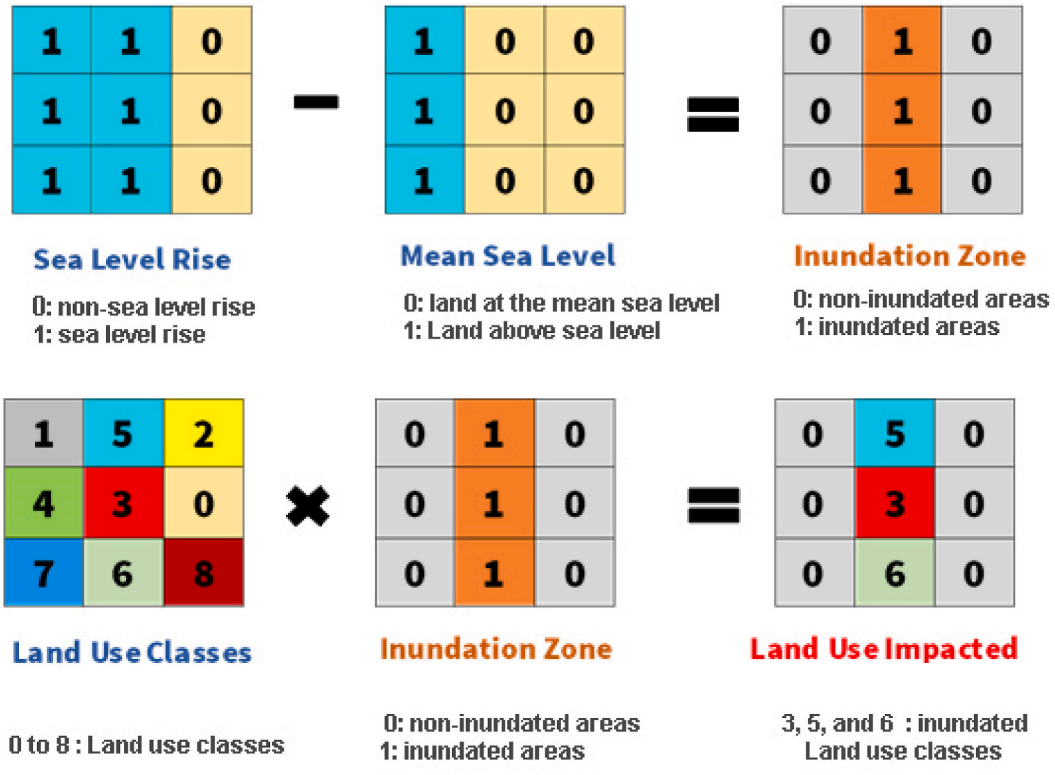

Fig. 3. Simple illustration depicting the relationship between SLR and the impacted areas of land use.

3.3. Digital elevation model

The Shuttle Radar Topography Mission (SRTM) was a collaborative project between NASA and international partners, launched in 2000 aboard the Space Shuttle Endeavour, with the goal of collecting accurate topographic data of the Earth's surface using radar technology. SRTM collected global elevation data at a resolution of approximately 90 m, while higher-resolution data were gathered for select regions. In this study, the data collected by the SRTM were employed to assess the impact of SLR on land utilization in Jeddah Province.

3.4. Scenarios

The datasets obtained were analyzed to determine the trend of SLR during the measurement period (2012–2021). Although these datasets are insufficient to establish a long-term trend, they offer insights into the climate behavior during the measuring period. The hourly data were converted to annual mean values for sea level rise, which were then analyzed to ascertain the mean annual SLR. The local SLR was estimated by calculating the mean sea level in the region, which was found to be 7.7 mm/year. This figure was obtained by dividing the value of 0.61255 (derived from regression analysis) by 79 years. Considering the non-linear growth in temperature for each SSP scenario, this value was used to estimate the SLR, as depicted in Table 2. It was also used to project the expected SLR (Table 2). Based on the anticipated temperature rise stipulated in the SSP scenario of the UN Intergovernmental Panel on Climate Change (IPCC) report from 2021, the mean SLR in Jeddah is projected to reach 1.01 m by the year 2100. In addition to the projected 2100 SLR, this study also considers three scenarios of 2, 5, and 10 m SLR to gain a better understanding of how Jeddah Province might respond to significant natural disasters, such as tsunamis.

3.5. Land use mapping

Land use mapping is the process of creating a spatial representation of how land is being used in a given area. Utilizing land use maps serves multiple objectives, including city development, ecological administration, and preservation of natural resources. Employing supervised land use and land cover (LULC) categorization is a prevalent technique in remote sensing and GIS for identifying and charting various LULC categories within a specified region [71,72].

For this study, real databases of LULC were required to better assess the impact of SLR on various infrastructures. These can be obtained from the General Authority for Survey and Geospatial Information (GASGI) [59]. GASGI is mandated to create and maintain a national geospatial database and to provide mapping and surveying services to government agencies and private sector entities. Additionally, the organization advocates for the implementation of geospatial technology and data to support economic development, environmental management, and national security. Operating under the Ministry of Municipal and Rural Affairs, GASGI collaborates closely with other government agencies, such as the Ministry of Defense and the Ministry of Interior, to support their surveying and mapping needs. The organization also works with international partners to enhance its geospatial capabilities and promote the use of geospatial information for global development [73]. The obtained GIS databases regarding land use were categorized into three types of infrastructure: green, built-up and road, and industrial. To enhance understanding of the study area, several maps were also produced:

Hillshade map: This map simulates the effect of illumination on a terrain surface in a geographic area. It is created by using a DEM to calculate the angle and direction of the terrain slope, then simulating the shading effect of the sun or other light source on the terrain surface [74].

Aspect map: This map represents the orientation of the terrain surface in a geographic area. Created by analyzing the slope of the terrain surface and calculating the direction that the slope faces for each cell in a raster dataset [75], each cell is assigned a value representing the direction the slope faces, typically in degrees. For example, a cell with an aspect value of 0° faces north, while a cell with an aspect value of 180° faces south. These maps are used in conjunction with other terrain variables, such as slope and elevation, to provide broader insight into the landscape's ecological and hydrological characteristics [75].

Distance to the river map: This map represents the distance of each point or cell in a geographic area to the nearest river or stream. Created by calculating the Euclidean or network distance from each point to the nearest river or stream using a raster or vector dataset of the river network, these maps can help in identifying suitable locations for infrastructure development while minimizing environmental impact. They also aid in identifying areas needing zoning or conservation measures to protect water quality and other ecological values [72].

Topographic Position Index (TPI): TPI is a quantitative measure used to characterize the local topographic variation of a landscape.

Table 2
Projected temperature and SLR in 2100 [22].

Scenario	Best estimate (°C) in 2100	SLR (m) (min-max-mean)	Average projected annual SLR (mm) (min-max-mean)
SSP1-1.9	1.4	0.28–0.55-0.30	3.25–6.4-4.48
SSP1-2.6	1.8	0.32–0.62-0.42	3.7–7.2-5.25
SSP2-4.5	2.7	0.44–0.76-0.52	5.11–8.8-6.7
SSP5-8.5	4.4	0.63–1.01-0.78	7.3–11.7-9.78

It is calculated by subtracting the elevation of a specific point in a Digital Elevation Model (DEM) from the mean elevation of the surrounding area within a defined radius [76]. TPI is commonly used to identify landforms and landscape features, model hydrological processes, and identify areas that are susceptible to erosion and landslides.

Terrain Roughness Index (TRI): TRI measures the variation in elevation of a landscape, describing the relative roughness of the

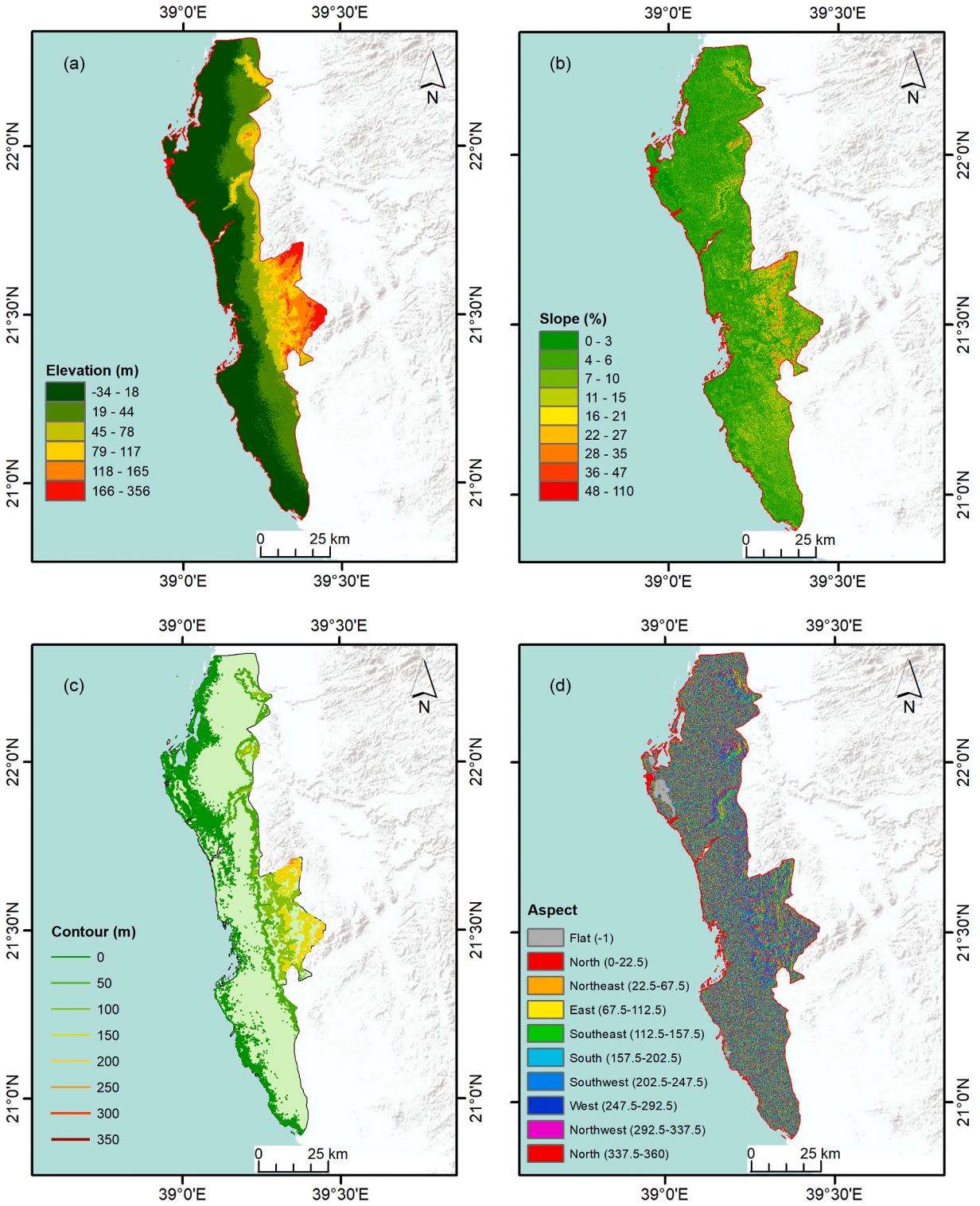

Fig. 4. Representation of (a) DEM, (b) slope, (c) contours, and (d) aspect of Jeddah Province.

terrain. Calculated by dividing the range of elevations within a specified radius by the radius itself [77], TRI values range between 0 (perfectly flat terrain) and 1 (extremely rugged terrain). It is commonly used to study the effects of topography on ecological and hydrological processes, to model water runoff, soil erosion, and to evaluate habitat suitability for various species.

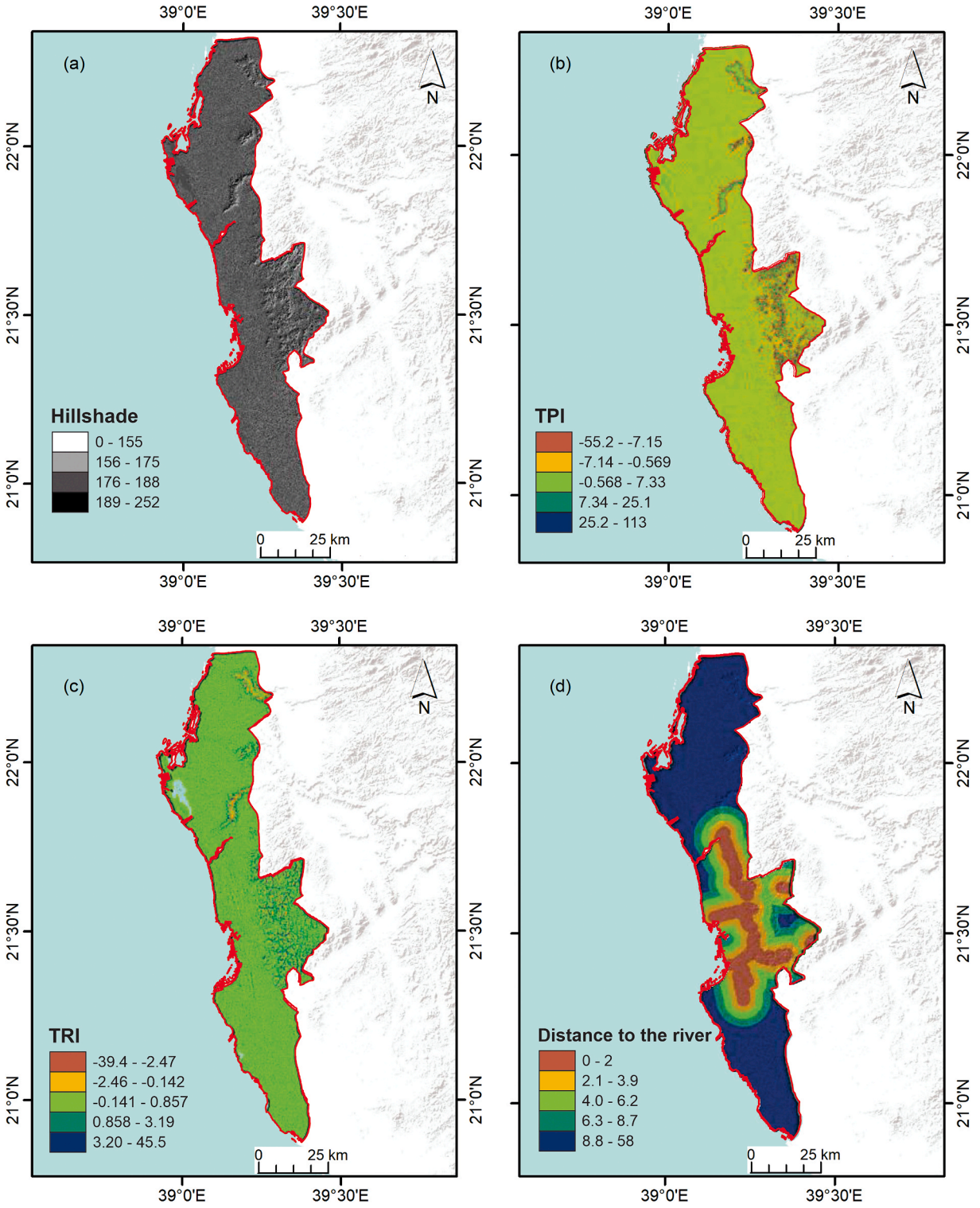

Fig. 5. Representation of (a) hillshade, (b) topographic position index (TPI), (c) terrain roughness index (TRI), and (d) distance to the river in Jeddah Province.

4. Results

The elevations within Jeddah Province range from −34 to 356 m as shown in (Fig. 4a). This DEM map suggests that the province may consist primarily of relatively flat or gently sloping terrain, with fewer areas of significant elevation changes or mountainous features when compared to other parts of the country. Fig. 4b further illustrates that the majority of higher elevations are localized within the eastern region of the province. Jeddah Province is characterized by slopes between 0 and 16%, while the extreme eastern part is dominated by steeper slopes reaching up to 109%. This region includes the mountains and plateaus of Hijaz. Notable among these are Umm Al-Rayhan, Quant Heights, Abu Ghasha, Al-Malees Plateau, Umm Raqiba, Mars Mountains, Al-Qarfa Mountains, Green Mountains, Umm Al-Salam Heights, and Muriha Mountain. Their contours range from 200 to 350 m as depicted in Fig. 4c. Jeddah, situated between these two mountain regions, is more influenced by terrain factors compared to cities located above the mountains. The eastern and western heights surrounding the city influence the climate of Jeddah. Fig. 4d demonstrates that the flat aspect dominates the province, rendering it vulnerable to flooding. This vulnerability was highlighted by the flood disaster that occurred in Jeddah in November 2009, causing significant material and human damage. Additionally, in November 2022, widespread flooding occurred in most parts of the coastal city due to heavy rains and thunderstorms. This led to the inundation of many streets and the closure of several major roads, including the main highway between Jeddah and Makkah.

The Hillshade map (Fig. 5a) simulates the illumination of the terrain by calculating light intensity values for each cell within a grid. This process involves determining the position of a hypothetical light source and computing lighting values for each cell in relation to its neighboring cells. Shading significantly enhances the visualization of a plane when displaying analyses or diagrams, especially when utilizing transparency [78]. For Jeddah Province, most Hillshade values fall within the range of 155 to 188 (Fig. 5a). The TPI of the study area (Fig. 5b) aids in distinguishing topographic features such as valley bottoms, hilltops, flat plains, exposed ridges, and lower or upper slopes. TPI is computed by comparing the altitude of each pixel with those of its adjacent neighbors. It is often used in predicting wetland distributions [79], assessing the relationship between soil and landform in glacial-drift areas [54], and evaluating urban green spaces [80]. Negative values represent valley bottoms (depressions), while positive values signify hilltops and exposed ridges, mapping elevated areas (Fig. 5b). Moreover, TPI values approaching zero may indicate regions with minimal incline (with slopes close to zero) or zones with consistent gradients (where the slope at a particular point is significantly more than zero) [81] (Fig. 5b). The Topographic Roughness Index (TRI) (Fig. 5c), the average of elevation discrepancies between a central grid cell and its surrounding cells (measured in meters), assesses terrain heterogeneity. The results may resemble those of the slope, but roughness emphasizes the discontinuities in relief [82,83]. The modal range of TRI values usually falls between −39 and 45. Within this range, the dominant TRIs are often low values, typically less than "3," indicating relatively smooth terrain characteristics across the study region (Fig. 5c). However, exceptions exist, particularly in the southwestern area of the study region where high mountains are found (Fig. 5c). Some of the most prominent valleys include Wadi Bani Malik, Wadi Comfortable, Wadi Al Qaws, Ashir, and Abu Nabaa. Therefore, Jeddah is considered to be situated in one of the valley bottoms, making it vulnerable to flood destruction. Fig. 5d illustrates

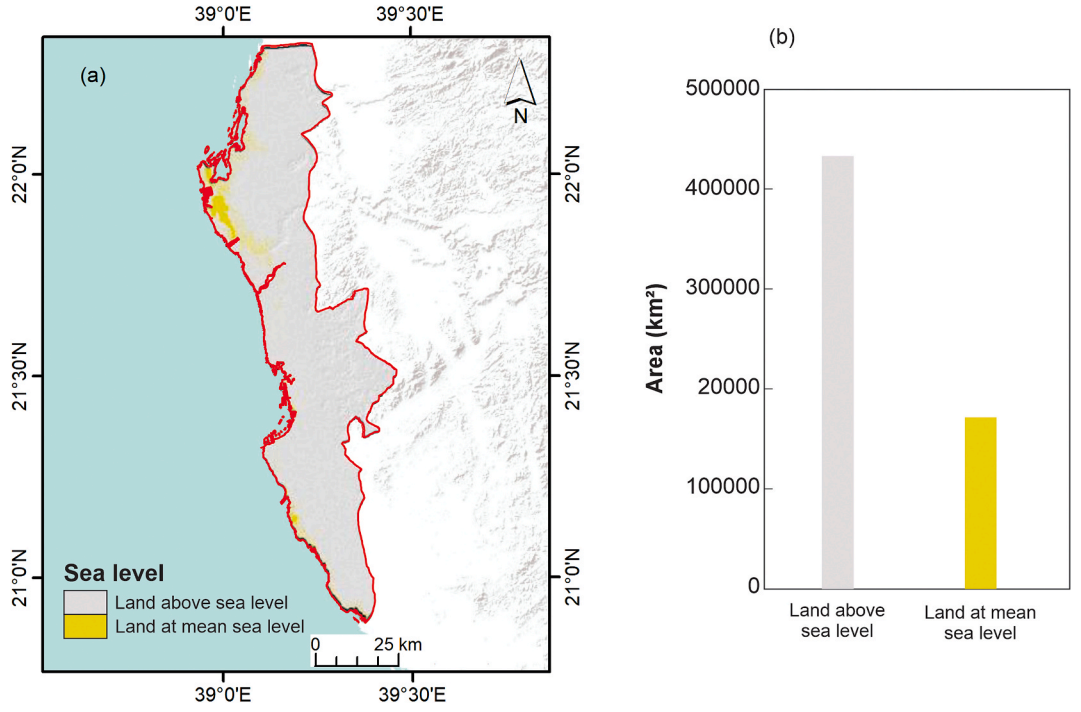

Fig. 6. (a) Mapping of areas above sea level and areas at sea level, and (b) bar graph illustrating the areas above sea level and areas at mean sea level.

the distance to the river in the study area. Urban areas located adjacent to the banks of valleys are generally deemed unsuitable for construction due to several factors, including a higher risk of flooding, unstable soils, and an increased vulnerability to landslides.

Based on the raster calculator, areas with an elevation of less than or equal to zero meters can be found. Fig. 6a displays the mapping of areas above sea level and those at sea level. In the present case, the number "0" represents "Land above sea level," and the number "1" corresponds to "Land at the mean sea level" (Fig. 6a). Based on the findings, the area at the mean sea level is approximately 165 km^2, whereas the area above sea level is 4405 km^2 (Fig. 6b).

The results of mapping various SLR scenarios of 1 m (projected), 2, 5, and 10 m for the Jeddah Province are illustrated in Fig. 7a, b, and c. To determine how much land is inundated by the rising water level, one must subtract the Mean Sea Level raster from the different sea level rise rasters, as explained in Fig. 3. The result is a raster model representing strips of land along the coast that will be flooded by an SLR of 1 m (Fig. 8a), 2 m (Figs. 8b), 5 m (Fig. 8c), and 10 m (Fig. 8d). Here, the pixels with a value of 1 are the water or "inundated areas," and the pixels with a value of 0 are the land or "non-inundated areas" (Fig. 8). As shown in Fig. 9, the inundated areas for various SLRs range from 1.6 to 30.6%, or 88.3 to 1398 km^2, of Jeddah Province's total area. The results of the SLR of 1 m impact revealed that 1.6% or 88 km^2 of the coast of the study area might be inundated (Figs. 8a and 9a, b). The SLR of 2 m indicated that 4.7% (214 km^2) of the coast region of Jeddah Province could be seen as inundated areas (Figs. 8b and 9a, b). In comparison, 679 km^2 (14.9%) of land along the coast can be inundated with an SLR of 5 m (Figs. 8c and 9a, b). More than 1398 km^2, explaining 30.6% of the study area, can be inundated if the SLR equals 10 m (Figs. 8d and 9a, b).

In order to accurately assess the impacts of 1, 2, 5, and 10 m of SLR on the civil engineering, agriculture, and industrial infrastructures of Jeddah Province, it is crucial to use land-use databases and GIS layers obtained from GASGI. These data can be incorporated into a decision-making tool, which can be used to evaluate economic loss for each SLR scenario. Additionally, this tool can provide valuable information for future planning of the civil engineering infrastructure in Jeddah Province.

Numerous methods have been employed in the literature to obtain land use change (LUC) maps, such as LUC analysis based on Landsat databases and supervised maximum likelihood classification methods, in conjunction with GIS technologies [72,84,85]. However, these studies require real data to comprehensively assess the SLR impacts on land use. Recognizing the importance of geospatial information in decision-making and its role in influencing the quality of life and achieving the 2030 sustainable development plans, KSA has been committed to covering the primary domains associated with geographic data. This encompasses developments in geospatial data management, upcoming digital frameworks, AI, large datasets, analytical information, emerging trends in data generation, policy, and legal development, necessary skills and training approaches, the involvement of private and non-governmental organizations, and the evolving responsibilities of governments in supplying and handling geospatial data, along with the needs of potential users [86].

Geospatial information is fundamental to Saudi Arabia's Vision 2030, as highlighted in the section "Protecting the environment from natural hazards." The vision includes addressing issues such as desertification, torrential rains, sandstorms, and the spread of epidemics, and reducing the losses caused by sandstorms, floods, and inundations. Achieving these goals involves increasing the accuracy of forecasts and early warnings for such events [87].

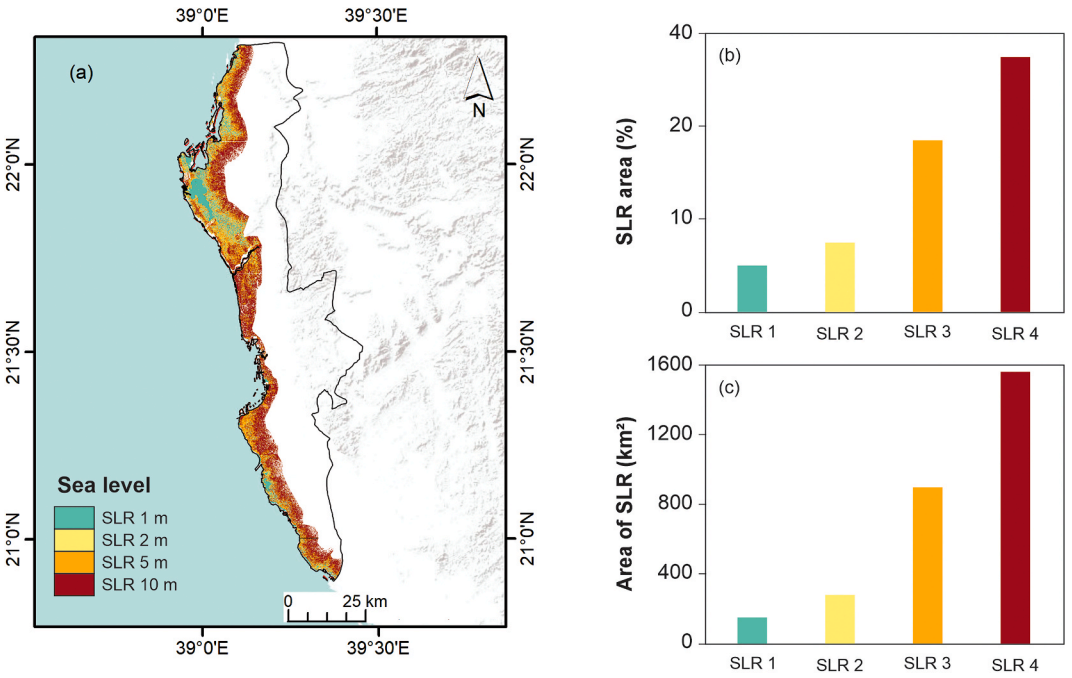

Fig. 7. (a) Mapping of projected SLR scenarios of 1 m, 2 m, 5 m, and 10 m for the study area, with the corresponding areas shown as a (b) percentage and (c) in kilometers square.

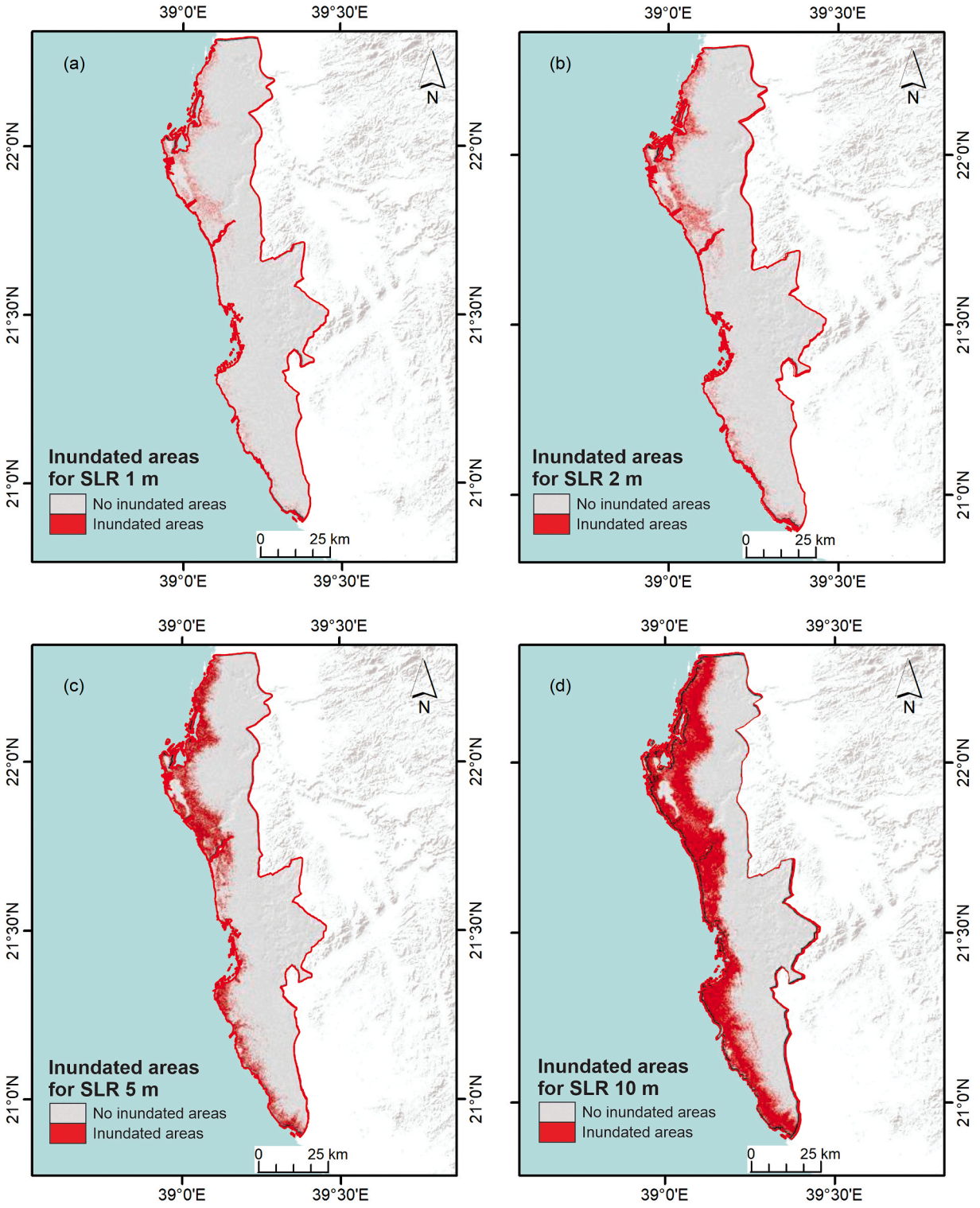

Fig. 8. Mapping of inundated and non-inundated areas in Jeddah Province for the various SLRs.

The KSA's GASGI has established the National Geospatial Platform, which enables users to access a diverse range of national geospatial data layers relevant to areas such as planning, development, agriculture, transportation, security, societal aspects, health, education, culture, commerce, and land utilization. The platform includes an interactive interface and statistical information, and is compatible with multiple GIS applications [88,89].

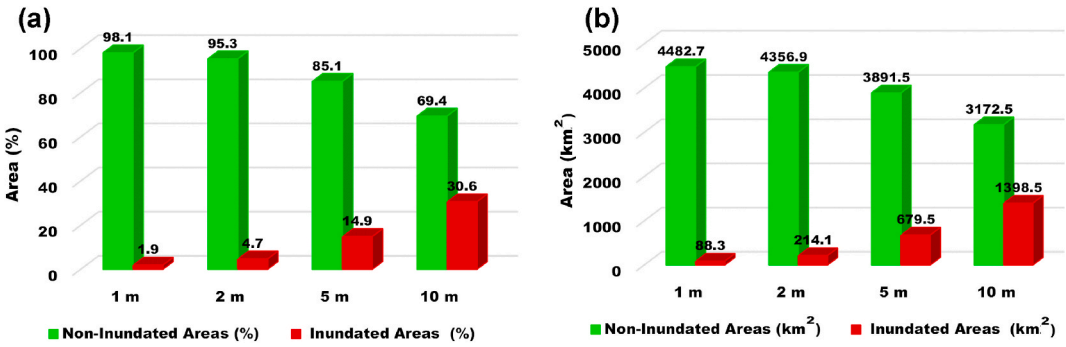

Fig. 9. Area of inundated and non-inundated areas in (percentage) and (km^2) at Jeddah Province for the various SLRs.

The innovation of our research lies in the utilization of extensive databases, divided into three distinctive types of infrastructure: green, built-up and road, and industrial. The green infrastructure encompasses farms, forests, grassland meadows, orchards, recreation grounds, and scrubland. The category of built-up and road infrastructure incorporates buildings, roads, allotments, parks, cemeteries, and spaces for military, commercial, residential, and retail purposes. Finally, the industrial infrastructure comprises industrial zones and quarries. It is noteworthy to mention that Jeddah houses 750 factories, making up 23.58% of the total count of factories throughout the Kingdom's regions.

The inundation rasters consist of pixel values that are either 1 or 0, as represented in Fig. 8. The land use raster is composed of pixel values from 1 to 3. These numbers represent different land-use types: the first class includes green infrastructures, the second built-up and road infrastructures, and the third industrial infrastructures. The impact of SLR on the different land-use categories was determined by multiplying the two raster datasets. Any pixel from the land-use raster multiplied by a 0 on the inundation raster becomes a 0, and any pixel from the land-use raster multiplied by a 1 on the inundation raster retains its original value, as explained in Fig. 3. The result is a raster layer with numbers 1 through 3 representing the land-use categories impacted by SLR. The results of inundated and non-inundated land-use infrastructures in Jeddah Province for various SLRs are illustrated in Fig. 10.

Transportation and road networks are essential elements that can be used to measure the extent of development and interdependence of the urban field with all its features. The results revealed that the 1 m SLR influences 1.3% of the total road length. Approximately 3.3% of the road length can be flooded by a 2 m SLR scenario, and this figure can reach 14% in the case of a 5 m SLR. Furthermore, the scenario of a 10 m SLR can inundate approximately 34% of the total road length (Figs. 10 and 11).

The impact assessments of 1, 2, 5, and 10 m SLRs on various land-use infrastructures indicate that 1 and 2 m of SLRs do not substantially affect the green, built-up and road, and industrial infrastructures of Jeddah Province (Fig. 10a, b, 11, 12, and 13). The land-use area of the aforementioned classes totals approximately 27 km^2. The non-inundated areas are approximately 25.97 km^2 (98.8%) and 25.48 km^2 (96.95%) for 1 and 2 m SLR, respectively. For 5 and 10 m SLRs, these areas decrease to 22.48 km^2 (85.9%) and 17.06 km^2 (65.16%), respectively (Fig. 12). The inundation impacts on built-up and road areas are estimated between 0.31 km^2 and 0.79 km^2, accounting for 1.18 to 3.01% of the total class area for 1 and 2 m SLRs, respectively. Meanwhile, the green and industrial infrastructure areas are not significantly affected, with inundation areas not exceeding 0.002 km^2 and 0.01 km^2 (0.01% and 0.04%) (Fig. 13). For a 5 m SLR, the built-up and road areas are the most impacted with an inundation area of 3.65 km^2 (13.96%). Industrial infrastructures rank second with an estimated inundation area of 0.03 km^2 (0.11%), followed by green space infrastructures at 0.0086 km^2 (0.033%) (Fig. 13). In the case of 10 m SLR, inundation most significantly impacts the built-up and road infrastructure areas, estimated at 8.9 km^2 (34%), while the industrial infrastructures are estimated to have an inundation area of 0.21 km^2 (0.78%), followed by green space infrastructures at 0.013 km^2 (0.051%) (Fig. 13).

5. Discussion

A primary objective within the six central aims of the vision is specifically tied to urban environments, with the intent to enhance city living standards. This objective is emphasized through the inclusion of one of the 13 initiatives designed to realize the vision, known as the "Quality of Life 2020″ program, which seeks to make progress in this area. It is anticipated that the Saudi Red Sea resort area will welcome visitors in 2023, and by 2030, the resort will encompass 50 hotels with 8,000 hotel units, up to 1,000 residential properties, as well as an international airport for the area [90]. The 1 m SLR impact results reveal that 1.6%, or 88 km^2, of the study area's coast may be inundated. In contrast, the inundated land-use analysis shows that the 1 m SLR influences 1.3% of the total road length, where 3.3% of road length can be flooded by a 2 m SLR scenario and can reach 14%. Furthermore, the assessment of different SLRs' impacts on land-use infrastructures reveals that 1 and 2 m SLRs do not significantly affect the land use of Jeddah Province. The non-inundated areas are estimated at 25.97 (98.8%) and 25.48 (96.95%) km2 for 1 and 2 m SLR, respectively. Overall, for the cases of 1 and 2 m SLRs, the study area is not significantly influenced, making it somewhat secure or protected from the danger of flooding, especially at present. Conversely, the losses will be significant for 5 and 10 m SLRs.

The results obtained from this study align with those from Ref. [91], which analyzed the impact of a 1 m SLR scenario on the coastal districts of Jeddah, Saudi Arabia. Khusaifan's findings showed minimal intrusion impacts from a 1 m SLR, with less than 10% of the

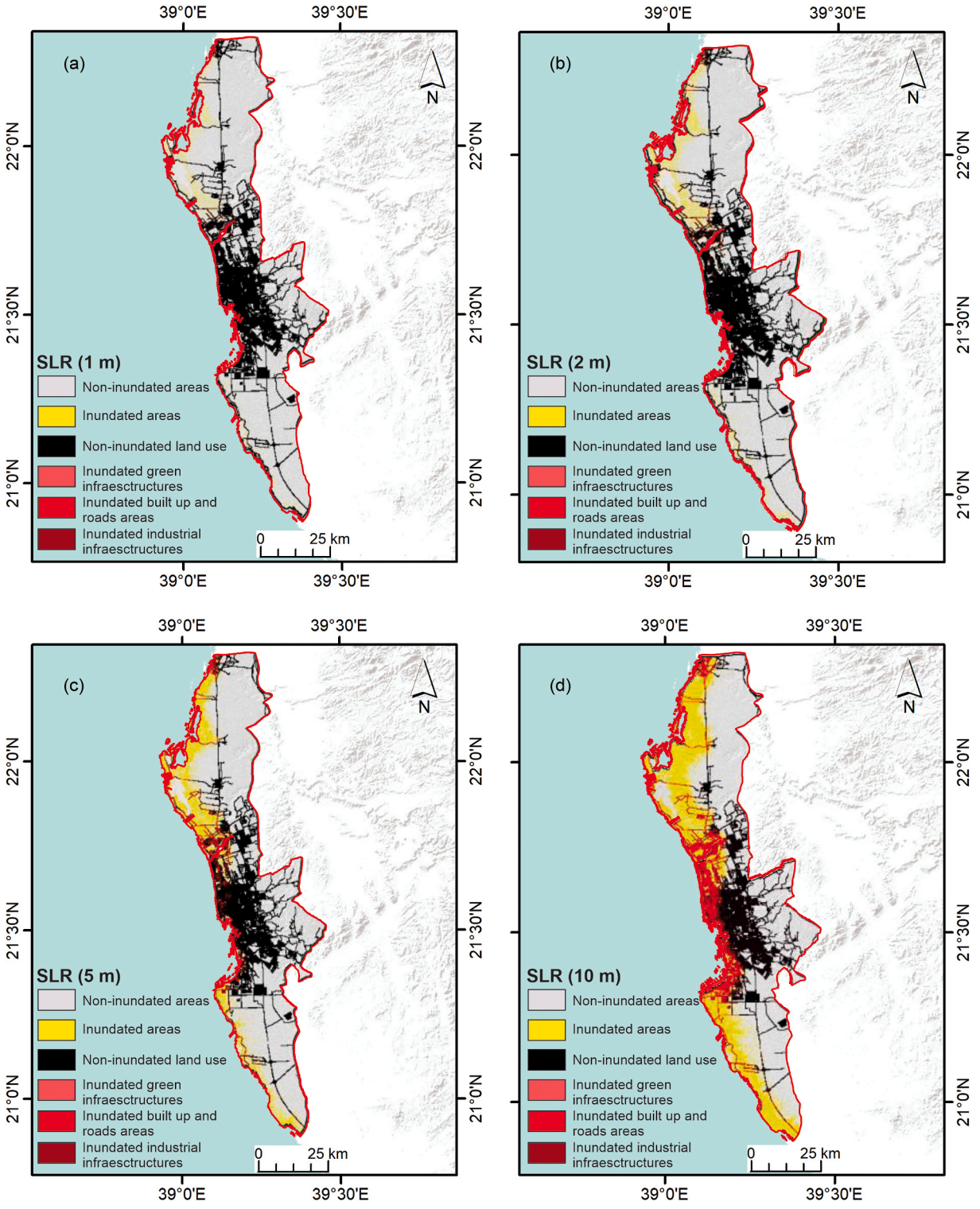

Fig. 10. Variations in inundated across different land-use infrastructures in Jeddah Province at various SLRs.

total district area (7 out of 24 districts) being affected. Contrarily, a technical report by Ref. [92] identified the coastal cities of Saudi Arabia—Jeddah, Yanbu, Rabigh, and Gizan, all located along the Red Sea shoreline—as the most vulnerable to accelerated SLR. Ref. [93] conducted an assessment of the Red Sea shoreline's vulnerability to climate change impacts in Saudi Arabia. The DEM analysis results showed that approximately 890 km^2 of the coastline is located at elevations below 1 m. The Coastal Vulnerability Index

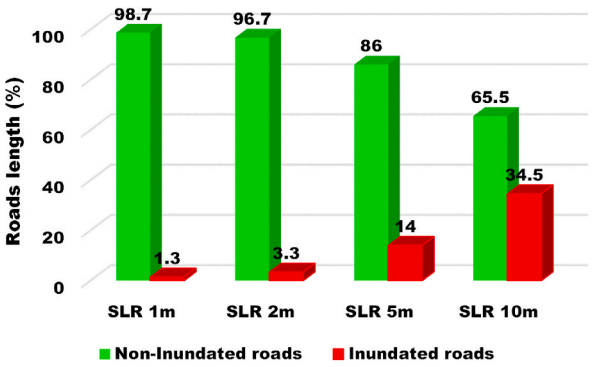

Fig. 11. Area of inundated and non-inundated roads in percentage at Jeddah Province for the various SLRs.

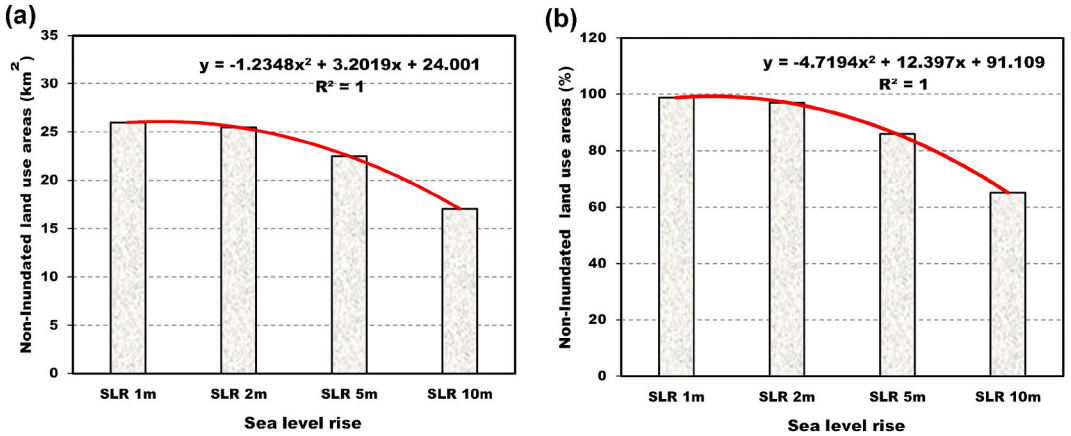

Fig. 12. Non-inundated area of various land-use infrastructures in percentage and km^2 at Jeddah Province for the various SLRs.

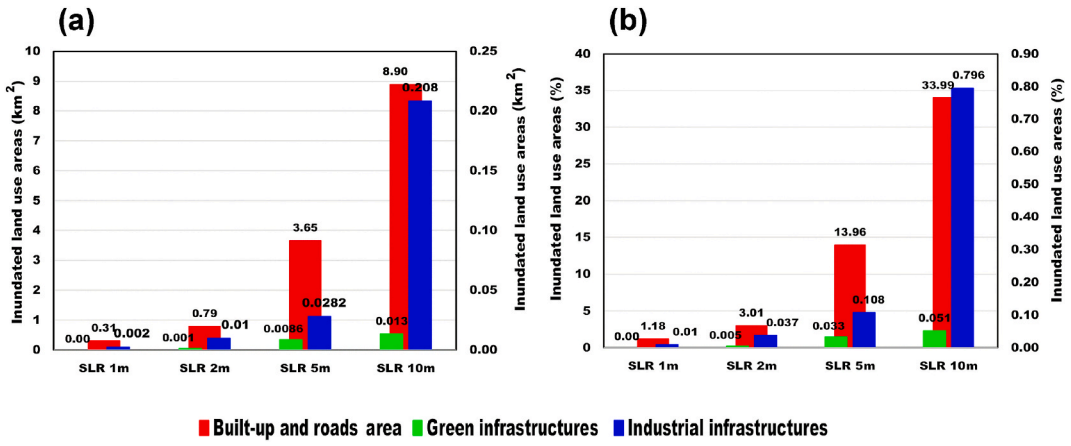

Fig. 13. Inundated Area OF various land-use infrastructures in percentage and km^2 at Jeddah Province for the various SLRs.

(CVI) indicated high vulnerability values for approximately 16% of the coast, while about 44% demonstrated a significantly low level of vulnerability. Areas with elevated risks typically exhibit dense populations, flat terrains, and low-lying regions. In the Yanbu region of Saudi Arabia, Aina and Aleem [94] evaluated an industrial city's vulnerability to SLR using GPS observations and SRTM databases. Their analysis revealed that the city would be vulnerable to a 1 m SLR by the year 2100. Additionally, Ref. [95] simulated SLR and its impacts on the western coastal area of Saudi Arabia, noting that the area under study is highly sensitive to changes in SLR. The insights gained from mapping SLR in Jeddah Province could be instrumental for future decision-making and planning processes. These findings

can provide valuable spatial information that can be used to construct better civil engineering structures within the scope of sustainable development.

The results obtained in this study are of critical importance for decision-makers in Jeddah Province for the following reasons:

1. Understanding Climate Change: SLR is one of the most significant consequences of climate change. Studying SLR allows scientists to gain insights into the complex interactions between the atmosphere, oceans, and ice sheets, which can aid in understanding the broader implications of climate change on the Earth's systems.
2. Coastal Vulnerability: SLR poses a significant threat to coastal areas globally. It can lead to increased coastal erosion, inundation of low-lying areas, saltwater intrusion into freshwater sources, and more frequent and severe coastal flooding. Studying SLR helps assess the vulnerability of coastal communities, ecosystems, and infrastructure, thereby enabling policymakers and planners to make informed decisions about adaptation and resilience.
3. Environmental Impact: SLR can adversely affect coastal ecosystems, including wetlands, estuaries, coral reefs, and mangroves. These ecosystems provide habitats for numerous species, help mitigate the impacts of storm surges, and support the livelihoods of coastal communities. SLR studies aid in understanding and predicting potential ecological consequences, thus facilitating conservation efforts and ecosystem management strategies.
4. Infrastructure Planning and Design: SLR studies are crucial for infrastructure planning and design in coastal regions. Accurate predictions of future sea levels inform decisions on the location, design, and construction of critical infrastructure such as buildings, roads, ports, and flood protection systems. By incorporating SLR projections into infrastructure planning, resilience is ensured, and long-term risks are reduced.
5. Policy Development: SLR studies provide the scientific basis for policy development and decision-making at various levels, from local to international. Governments and organizations rely on this research to develop strategies and policies related to coastal management, land-use planning, disaster preparedness, and climate change mitigation and adaptation.
6. International Cooperation: SLR is a global challenge that requires international collaboration and coordination. SLR studies facilitate knowledge sharing, data exchange, and collaborative efforts among scientists, policymakers, and stakeholders worldwide. They contribute to global initiatives like the IPCC, which assesses and synthesizes scientific knowledge to inform international climate policies.

Implementing research on the impact of sea level rise on land use can pose several challenges. Some of the commonly faced challenges, along with potential ways to overcome them, are (1) data availability: gathering comprehensive and reliable data on both SLR and land use can be challenging. Historical data may be limited, and projections for future sea level rise can vary significantly; (2) interdisciplinary approach: studying the impact of SLR on land use requires expertise from various disciplines, including climatology, geology, geography, ecology, and urban planning; (3) complex dynamics: the relationship between SLR and land use is complex and influenced by numerous factors, such as coastal geomorphology, socioeconomic conditions, and governance. Overcoming this challenge involves developing robust modeling techniques that incorporate multiple variables and their interactions; (4) uncertainty and future projections: predicting the future impacts of SLR on land use involves inherent uncertainties. This challenge can be addressed by acknowledging and quantifying uncertainties in data, models, and projections; and (5) stakeholder engagement: implementing research findings and ensuring their practical application require collaboration and engagement with stakeholders, including local communities, policymakers, and relevant organizations. This is arguably one of the most critical challenges.

6. Conclusion

This study demonstrated the effects of 1-meter, 2-meter, 5-meter, and 10-meter SLRs on Jeddah Province (KSA) using DEM, the eight-side rule algorithm implemented in GIS, and observed measurements of tidal levels taken every hour during the 2012–2021 period. Hourly tide gauge measurements were analyzed to define the study area's annual sea level rise rate. The study concluded the following points:

- The findings from the SLR impacts of 1, 2, 5, and 10 m revealed that 1.6, 4.7, 14.9, and 30.6% (or 88, 214, 679, 1398 km^2) of the coast in the region under consideration could be classified as inundated areas.
- The results revealed that the projected 2100 1-meter SLR influences 1.3% of the total road area/length. Moreover, 2-meter, 5-meter, and 10-meter SLR scenarios can inundate 3.3 to 34% of the road area/length.
- The assessment of different SLRs' impacts on land-use infrastructures revealed that 1-meter and 2-meter SLRs could not significantly affect the land use of Jeddah Province. The non-inundated areas were estimated at 25.97 (98.8%) and 25.48 (96.95%) km^2 for 1-meter and 2-meter SLRs, respectively. The non-inundated area can decrease to 22.48 (85.9%) and 17.06 (65.16%) km^2 for 5-meter and 10-meter SLRs, respectively.
- The inundated built-up and road areas were estimated between 0.31 and 0.79 (km^2), which accounts respectively for 1.18 to 3.01% of the total class areas for 1-meter and 2-meter SLRs.
- Furthermore, the green space and industrial infrastructure areas were inundated by small areas for SLR less than 5 m.
- In the case of 10 m SLR, the inundation will negatively influence the built-up and road infrastructure areas, inundating 8.9 km^2. In contrast, the industrial infrastructures impacted by inundation were estimated at 0.21 km^2, followed by green space infrastructures at 0.013 km^2.

These results suggest the necessity for adaptation or mitigation actions to reduce economic losses, avoid shoreline retreats, and prevent relocation plans for vulnerable populations in Jeddah Province's coastal zone. The developed maps could provide invaluable assistance to decision-makers and planners for future decisions concerning the construction of civil engineering structures within the framework of sustainable development. However, this study has some potential limitations. One limitation is its focus on a general assessment of SLR impacts on Jeddah city, which might overlook some specific localized effects. Another significant limitation relates to the LULC data, which may not always offer a high spatial resolution. Consequently, fine-scale details and changes in land cover might not be accurately captured. The accuracy of LULC classifications can also vary as it depends on remote sensing techniques and the interpretation of satellite imagery. Inaccurate or outdated LULC data can introduce uncertainties in SLR studies and subsequent vulnerability assessments. Furthermore, this study does not provide an accurate estimation of material losses. While the bathtub approach, used in this study, offers simplicity, it oversimplifies the complex nature of SLR impacts. It neglects local factors and vulnerabilities, potentially leading to inaccurate predictions and inadequate adaptation planning. Future research will be directed toward a combined analysis using advanced techniques such as Synthetic Aperture Radar (SAR) and machine learning. These methods could enhance the accuracy and effectiveness of SLR analysis, provide high spatial resolution, improve change detection, better identify vulnerable areas, and strengthen the evidence base for policy development and urban planning. This will allow for the consideration of SLR risks and the minimization of potential damages.

Author contribution statement

Abdulrazak H. Almaliki; Bilel Zerouali; Celso Augusto Guimarães Santos: Conceived and designed the experiments; Performed the experiments; Analyzed and interpreted the data; Contributed reagents, materials, analysis tools or data; Wrote the paper. </p>

Abdulrhman A. Almaliki; Richarde Marques da Silva; Sherif S. M. Ghoneim; Enas Ali: Analyzed and interpreted the data; Contributed reagents, materials, analysis tools or data; Wrote the paper. </p>

Data availability statement

Data will be made available on request.

Funding

The researchers would like to acknowledge the Deanship of Scientific Research, Taif University for funding this work.

Declaration of competing interest

The authors declare that they have no known competing financial interests or personal relationships that could have appeared to influence the work reported in this paper.

Acknowledgments

The researchers would like to acknowledge the Deanship of Scientific Research, Taif University for funding this work.

References

[1] F. Laila, Assessment on social vulnerabilities to climate change—a study on south-western coastal zones of Bangladesh, master's thesis, E, in: Sustainable Development, Department of Earth Sciences, Uppsala University, Uppsala, Sweden, 2013.
[2] B. Zerouali, A. Elbeltagi, N. Al-Ansari, Z. Abda, M. Chettih, C.A.G. Santos, A.S. Araibia, Improving the visualization of rainfall trends using various innovative trend methodologies with time–frequency-based methods, Appl. Water Sci. 12 (9) (2022) 207, https://doi.org/10.1007/s13201-022-01722-3.
[3] A. Elbeltagi, B. Zerouali, N. Bailek, et al., Optimizing hyperparameters of deep hybrid learning for rainfall prediction: a case study of a Mediterranean basin, Arabian J. Geosci. 15 (2022) 933, https://doi.org/10.1007/s12517-022-10098-2.
[4] N. Beg, J.C. Morlot, O. Davidson, Y. Afrane-Okesse, L. Tyani, F. Denton, Y. Sokona, J.P. Thomas, E.L. La Rovere, J.K. Parikh, K. Parikh, A.A. Rahman, Linkages between climate change and sustainable development, Clim. Pol. 2 (2–3) (2002) 129–144, https://doi.org/10.3763/cpol.2002.0216.
[5] J.S. Damtoft, J. Lukasik, D. Herfort, D. Sorrentino, E.M. Gartner, Sustainable development and climate change initiatives, Cement Concr. Res. 38 (2) (2008) 115–127, https://doi.org/10.1016/j.cemconres.2007.09.008.
[6] J.M. Gregory, J. Oerlemans, Simulated future sea-level rise due to glacier melt based on regionally and seasonally resolved temperature changes, Nature 391 (6666) (1998) 474–476, https://doi.org/10.1038/35119.
[7] P.G. Kovadlo, A.Y. Shikhovtsev, S.A. Yazev, The role of glaciers in the processes of climate warming, Atmosph. Oceanic Optics 35 (4) (2022) 434–438, https://doi.org/10.1134/S1024856022040091.
[8] C.R. Stokes, N.J. Abram, M.J. Bentley, T.L. Edwards, M.H. England, A. Foppert, S.S.R. Jamieson, R.S. Jones, M.A. King, J.T.M. Lenaerts, B. Medley, B.W.J. Miles, G.J.G. Paxman, C. Ritz, T. van de Flierdt, P.L. Whitehouse, Response of the east antarctic ice sheet to past and future climate change, Nature 608 (7922) (2022) 275–286, https://doi.org/10.1038/s41586-022-04946-0.
[9] J.E. Box, A. Hubbard, D.B. Bahr, W.T. Colgan, X. Fettweis, K.D. Mankoff, A. Wehrlé, B. Noël, M.R. van den Broeke, B. Wouters, A.A. Bjørk, R.S. Fausto, Greenland ice sheet climate disequilibrium and committed sea-level rise, Nat. Clim. Change (2022), https://doi.org/10.1038/s41558-022-01441-2.
[10] S. Dangendorf, C. Hay, F.M. Calafat, M. Marcos, C.G. Piecuch, K. Berk, J. Jensen, Persistent acceleration in global seasea-level rise since the 1960s, Nat. Clim. Change 9 (9) (2019) 705–710, https://doi.org/10.1038/s41558-019-0531-8.
[11] A. Eliawa, A. Numanoğlu Genç, H. Tora, H.H. Maraş, Risk assessment of Sea Level rise for karasu coastal area, Turkey, Hydrology 10 (2023) 13, https://doi.org/10.3390/hydrology10010013.

[12] IPCC. Managing the risks of extreme events and disasters to advance climate change adaptation, in: C.B. Field, V. Barros, T.F. Stocker, D. Qin, D.J. Dokken, K. L. Ebi, M.D. Mastrandrea, K.J. Mach, G.-K. Plattner, S.K. Allen, et al. (Eds.), A Special Report of Working Groups I and II of the Intergovernmental Panel on Climatic Change, IPCC, Cambridge, UK.; New York, NY, USA, 2012, p. 582.

[13] M.E. Hauer, E. Fussell, V. Mueller, M. Burkett, M. Call, K. Abel, R. McLeman, D. Wrathall, Sea-level rise and human migration, Nat. Rev. Earth Environ. 1 (1) (2020) 28–39, https://doi.org/10.1038/s43017-019-0002-9.

[14] S. Fagherazzi, S.C. Anisfeld, L.K. Blum, E.V. Long, R.A. Feagin, A. Fernandes, W.S. Kearney, K. Williams, Sea level rise and the dynamics of the marsh-upland boundary, Front. Environ. Sci. 7 (2019), https://doi.org/10.3389/fenvs.2019.00025.

[15] I.A. Elshinnawy, A.H. Almaliki, Vulnerability assessment for Sea Level rise impacts on coastal systems of gamasa ras el bar area, nile delta, Egypt, Sustainability 13 (2021) 3624, https://doi.org/10.3390/su13073624.

[16] J.A. Church, N.J. White, Sea-level rise from the late 19th to the early 21st century (open access), Surv. Geophys. 32 (2011) 585–602, https://doi.org/10.1007/s10712-011-9119-1.

[17] F.M. Calafat, D.P. Chambers, M.N. Tsimplis, On the ability of global sea level reconstructions to determine trends and variability, J. Geophys. Res. Ocean. 119 (2014) 1572–1592, https://doi.org/10.1002/2013JC009298.

[18] A.B.A. Slangen, J.A. Church, C. Agosta, X. Fettweis, B. Marzeion, K. Richter, Anthropogenic forcing dominates global Mean Sea-level rise since 1970, Nat. Clim. Change 6 (2016) 701–705, https://doi.org/10.1038/nclimate2991.

[19] T. Frederikse, F. Landerer, L. Caron, S. Adhikari, D. Parkes, V.W. Humphrey, S. Dangendorf, P. Hogarth, L. Zanna, L. Cheng, Y.H. Wu, The causes of sea-level rise since 1900, Nature 584 (7821) (2020) 393–397, https://doi.org/10.1038/s41586-020-2591-3.

[20] IPCC. Intergovernmental Panel on climatic change in the eastern mediterranean basin, in: D.J. Stanley, F.C. Wezel (Eds.), Geological Evolution of the Mediterranean Basin, Springer, New York, NY, USA, 1994, pp. 249–269.

[21] IPCC. Intergovernmental, Panel on Climate Change Climate Change Synthesis Report, 2014. Available online: https://www.ipcc.ch/site/assets/uploads/2018/02/AR5_SYR_FINAL_SPM.pdf. (Accessed 22 June 2021).

[22] V.P. Masson-Delmotte, P. Zhai, S.L. Pirani, C. Connors, S. Péan, N. Berger, Ipcc, 2021: Summary for policymakers, in: Climate change 2021: The physical science basis. contribution of working group i to the sixth assessment report of the intergovernmental panel on climate change, 2021.

[23] Z. Yang, B. Li, B. Nan, X. Dai, C. Peng, X. Bi, A Methodological framework for assessing pastoral socio-ecological system vulnerability: a case study of Altay Prefecture in Central Asia, Sci. Total Environ. 862 (2023), 160828, https://doi.org/10.1016/j.scitotenv.2022.160828.

[24] P. Roy, S.C. Pal, R. Chakrabortty, I. Chowdhuri, A.K. Saha, M. Shit, Effects of climate change and sea-level rise on coastal habitat: vulnerability assessment, adaptation strategies and policy recommendations, J. Environ. Manag. 330 (2023), 117187, https://doi.org/10.1016/j.jenvman.2022.117187.

[25] R. Ramakrishnan, P. Shaw, P. Rajput, Coastal vulnerability map of Jagatsinghpur District, Odisha, India: a satellite based approach to develop two-dimensional vulnerability maps, Reg. Stud. Mar. Sci. 57 (2022), 102747, https://doi.org/10.1016/j.rsma.2022.102747.

[26] K.J. Rao, P. Subraelu, T.P. Rao, B.H. Malini, R. Ratheesh, S. Bhattacharya, A.S. Rajawat, Ajai sea-level rise and coastal vulnerability: an assessment of Andhra Pradesh coast, India through remote sensing and GIS, J. Coast Conserv. 12 (2008) 195–207, https://doi.org/10.1007/s11852-009-0042-2.

[27] M.E. Hereher, Vulnerability of the Nile Delta to sea level rise: an assessment using remote sensing, Geomatics, Nat. Hazards Risk 1 (2010) 315–321, https://doi.org/10.1080/19475705.2010.516912.

[28] N. Van Sang, K. Van Long, T.T. Dung, L. Van Nguyen, B.C. Que, D. Van Mong, B.D. Quang, O.B. Andersen, N.R. Forsberg, D.T. Bui, Seafloor depth mapping of central Vietnam's Sea Area and its surrounding using gravity anomaly data and gravity geological method, Adv. Space Res. (2023), https://doi.org/10.1016/j.asr.2023.04.033.

[29] M.L. Kirwan, D. Walters, W.R. Reay, J.A. Carr, Sea level driven marsh expansion in a coupled model of marsh erosion and migration, Geophys. Res. Lett. 43 (2016) 4366–4373, https://doi.org/10.1002/2016gl068507.

[30] T.R. Anderson, C.H. Fletcher, M.M. Barbee, L.N. Frazer, B.M. Romine, Doubling of coastal erosion under rising Sea Level by mid-century in Hawaii, Nat. Hazards 78 (2015) 75–103, https://doi.org/10.1007/s11069-015-1698-6.

[31] D. Datta, S. Deb, Analysis of coastal land use/land cover changes in the Indian sunderbans using remotely sensed data, Geo-Spatial Inf. Sci. 15 (2012) 241–250, https://doi.org/10.1080/10095020.2012.714104.

[32] A. Alharthi, M.A. El-Sheikh, M. Elhag, A.A. Alatar, G.A. Abbadi, M. Faisal, I.A. Arif, A.A. Baeshen, E.M. Eid, Remote sensing of 10 years changes in the vegetation cover of the northwestern coastal land of Red Sea, Saudi Arabia, Saudi J. Biol. Sci. 27 (2020) 3169–3179, https://doi.org/10.1016/j.sjbs.2020.07.021.

[33] B. Zerouali, C.A.G. Santos, T.V.M.D. Nascimento, R.M. Da Silva, A cloud-integrated GIS for forest cover loss and land use change monitoring using statistical methods and geospatial technology over Northern Algeria, J. Environ. Manag. 341 (2023), 118029, https://doi.org/10.1016/j.jenvman.2023.118029.

[34] A. Parrott, W. Brooks, O.P. Harmar, K. Pygott, Role of rural land use management in flood and coastal risk management, J. Flood Risk Manag. 2 (2009) 272–284, https://doi.org/10.1111/j.1753-318x.2009.01044.x.

[35] H.L.F. Cooper, C.H. Fletcher, Q. Chen, M.M. Barbee, Sea-level rise vulnerability mapping for adaptation decisions using LiDAR DEMs, Prog. Phys. Geogr. 37 (2013) 745–766, https://doi.org/10.1177/0309133313496835.

[36] A. Hodgson, D. Peel, N.H. Kelly, Unmanned aerial vehicles for surveying marine fauna: assessing detection probability, Ecol. Appl. 27 (2017) 1253–1267, https://doi.org/10.1002/eap.1519.

[37] W. Tang, W. Zhan, B. Jin, M. Motagh, Y. Wang, Spatial variability of relative sea-level rise in tianjin, China: insight from InSAR, GPS, and tide-gauge observations, IEEE J. Sel. Top. Appl. Earth Obs. Rem. Sens. 14 (2021) 2621–2633, https://doi.org/10.1109/jstars.2021.3054395.

[38] A.U. Husnain, N. Mokhtar, N.M. Shah, M. Dahari, M. Iwahashi, A Systematic literature review (SLR) on autonomous path planning of unmanned aerial vehicles, Drones 7 (2023) 118, https://doi.org/10.3390/drones7020118.

[39] A.M. Al-Othman, I. Ahmed, Hydrogeological framework and its implication on water level rise in eastern ArRiyadh, Saudi Arabia, Environ. Earth Sci. 67 (2012) 1493–1502, https://doi.org/10.1007/s12665-012-1593-3.

[40] D.S. Babu, S. Sivalingam, T. Machado, Need for adaptation strategy against global sea level rise: an example from Saudi coast of Arabian gulf, Mitig. Adapt. Strategies Glob. Change 17 (2012) 821–836, https://doi.org/10.1007/s11027-011-9346-2.

[41] F. Khan, T.M. Khan, A. Ahmed, H.A. Afan, M. Sherif, A. Sefelnasr, A. El-Shafie, Complex extreme sea levels prediction analysis: karachi Coast case study, Entropy 22 (2020) 549, https://doi.org/10.3390/e22050549.

[42] V. Lai, A. Ahmed, Malek, H.A. Afan, R.K. Ibrahim, A. El-Shafie, A.H. El-Shafie, Modeling the nonlinearity of Sea Level oscillations in the Malaysian coastal areas using machine learning algorithms, Sustainability 11 (2019) 4643, https://doi.org/10.3390/su11174643.

[43] A.G. Parker, M.W. Morley, S.J. Armitage, M. Engel, A. Parton, G.W. Preston, H. Russ, P. Drechsler, Palaeoenvironmental and Sea Level changes during the holocene in eastern Saudi Arabia and their implications for neolithic populations, Quat. Sci. Rev. 249 (2020), 106618, https://doi.org/10.1016/j.quascirev.2020.106618.

[44] N.A.A.B.S. Bahari, A.N. Ahmed, K.L. Chong, V. Lai, Y.F. Huang, C.H. Koo, J.L. Ng, A. El-Shafie, Predicting sea level rise using artificial intelligence: a review, Arch. Comput. Methods Eng. (2023), https://doi.org/10.1007/s11831-023-09934-9.

[45] A.F. Aziz, N.H. Mardi, M.A. Malek, S.Y. Teh, M.N.N.C. Wil, A.H. Shuja, A. El-Shafie, P. Kumar, M. Sherif, A. Elshafie, Development of inundation maps along east coast of peninsular Malaysia due to predicted seaquake from manila trench, Appl. Water Sci. 13 (2023), https://doi.org/10.1007/s13201-022-01860-8.

[46] N. Al-Mutairi, M.M.M. Alsahli, M.I. El-Gammal, M.a.A. Ibrahim, R.M.A. Samra, Environmental and economic impacts of rising sea levels: a case study in Kuwait's coastal zone, Ocean Coast Manag. 205 (2021), 105572, https://doi.org/10.1016/j.ocecoaman.2021.105572.

[47] R.M.A. Samra, M.I. El-Gammal, N. Al-Mutairi, M.M.M. Alsahli, M.a.A. Ibrahim, GIS-based approach to estimate Sea Level rise impacts on Damietta coast, Egypt, Arabian J. Geosci. 14 (2021), https://doi.org/10.1007/s12517-021-06810-3.

[48] R.M.A. Samra, The use of cartographic modeling to assess the impacts of coastal flooding: a case study of port Said governorate, Egypt, Environ. Monit. Assess. 189 (2017), https://doi.org/10.1007/s10661-017-6152-7.

[49] M.E. Hereher, Vulnerability assessment of the Saudi arabian Red Sea coast to climate change, Environ. Earth Sci. 75 (2016) 30, https://doi.org/10.1007/s12665-015-4835-3.

[50] M.M. Fouda, M.A. Gerges, Implications of Climate Change in the Red Sea and Gulf of Aden Region: *an Overview UNEP Regional Seas Reports and Studies*, UNEP, 1994.
[51] A.J. Niang, Monitoring long-term shoreline changes along Yanbu, kingdom of Saudi Arabia using remote sensing and GIS techniques, J. Taibah Univ. Sci. 14 (2020) 762–776, https://doi.org/10.1080/16583655.2020.1773623.
[52] M.S. Hariri, M.K. Khalil, A.E. Rifaat, Assessment of the present status of the red sea coastal zone between Haql and Yanbu, Saudi Arabia, JKAU: Mar. Sci. 24 (2013) 115–131, https://doi.org/10.4197/Mar.24-2.8, 2013 A.D./1434 A.H.).
[53] PERSGA. State, Of the Marine Environment, Report for the Red Sea and Gulf of Aden, PERSGA: Jeddah, Saudi Arabia, 2016.
[54] V.S. Shamji, Tidal dynamics along the western coast of Saudi Arabia, the Red Sea, Int. J. Innovative Technol. Explor. Eng. 9 (2019) 280–284.
[55] A. Moatamed, Degradation of mangrove forests and coral reefs in the coastal area of the southwestern region of Saudi Arabia, Biogeogr. J. Integr. Biogeogr. 35 (2020) 71–89, https://doi.org/10.21426/B635046580.
[56] M. Daoudi, A. Niang, Flood risk and vulnerability of Jeddah city, Saudi Arabia, in: Recent Advances in Flood Risk Management, Intech Open, London, UK, 2019, https://doi.org/10.5772/IntechOpen.82073.
[57] M. Daoudi, A. Niang, Detection of shoreline changes in the city of Jeddah and its impact on the geomorphological system using remote sensing data (1951–2018), Arabian J. Geosci. 14 (2021) 1265, https://doi.org/10.1007/s12517-021-07605-2.
[58] A. Mezaien, J.C. Baltazar, June). Evaluating the performance of a passive architectural element in a hot-dry climate through natural ventilation and thermal impact analysis, in: Proceedings of the American Solar Energy Society National Conference: ASES SOLAR 2022, Springer International Publishing, Cham, 2022, pp. 171–183.
[59] Register for national geospatial platform, Available on: https://geoportal.gasgi.gov.sa/RegApp/Account/Registration?returnUrl=https%3A%2F%2Fgeoportal.gasgi.gov.sa%2Fportal%2Fapps%2Fsites%2F%23%2Fgasgi-geoportal. (Accessed 21 January 2023).
[60] A.P. Yunus, R. Avtar, S. Kraines, M. Yamamuro, F. Lindberg, C.S.B. Grimmond, Uncertainties in tidally adjusted estimates of sea level rise flooding (bathtub model) for the Greater London, Rem. Sens. 8 (5) (2016) 366, https://doi.org/10.3390/rs8050366.
[61] L.L. Williams, M. Lück-Vogel, Comparative assessment of the GIS based bathtub model and an enhanced bathtub model for coastal inundation, J. Coast Conserv. 24 (2) (2020) 23, https://doi.org/10.1007/s11852-020-00735-x.
[62] T.W. Gallien, B.F. Sanders, R.E. Flick, Urban coastal flood prediction: integrating wave overtopping, flood defenses and drainage, Coast. Eng. 91 (2014) 18–28.
[63] T.W. Gallien, N. Kalligeris, M.P.C. Delisle, B.X. Tang, J.T. Lucey, M.A. Winters, Coastal flood modeling challenges in defended urban backshores, Geosciences 8 (12) (2018) 450, https://doi.org/10.3390/geosciences8120450.
[64] J. Kovanen, J. Oksanen, T. Sarjakoski, Near real-time coastal flood inundation simulation with uncertainty analysis and GPU acceleration in a web environment, Comput. Geosci. 119 (2018) 39–48, https://doi.org/10.1016/j.cageo.2018.06.007.
[65] B. Poulter, P.N. Halpin, Raster modelling of coastal flooding from sea-level rise, Int. J. Geogr. Inf. Sci. 22 (2) (2008) 167–182, https://doi.org/10.1080/13658810701371858.
[66] B. Poulter, J. Goodall, P.N. Halpin, Applications of network analysis for adaptive management of artificial drainage system in landscapes vulnerable to sea level rise, J. Hydrol. 357 (2008) 207–217, https://doi.org/10.1016/j.jhydrol.2008.05.022.
[67] D.L. Passeri, S.C. Hagen, S.C. Medeiros, M.V. Bilskie, K. Alizad, D. Wang, The dynamic effects of sea level rise on low-gradient coastal landscapes: a review, Earth's Future 3 (2015) 159–181, https://doi.org/10.1002/2015ef000298.
[68] P.D. Bates, A.P.J. De Roo, A Simple raster-based model for flood inundation simulation, J. Hydrol 236 (2000) 54–77, https://doi.org/10.1016/S0022-1694(00)00278-X.
[69] D.B. Gesch, Analysis of lidar elevation data for improved identification and delineation of lands vulnerable to seasea-level rise, J. Coast Res. 10053 (2009) 49–58, https://doi.org/10.2112/si53-006.1.
[70] E.E. Lentz, E.R. Thieler, N.G. Plant, S.R. Stippa, R.M. Horton, D.B. Gesch, Evaluation of dynamic coastal response to sea-level rise modifies inundation likelihood, Nat. Clim. Change 6 (2016) 696–700, https://doi.org/10.1038/nclimate2957.
[71] R.Y. Shrahily, M.A. Alsharif, B.A. Mobarak, A.A. Alzandi, Land cover mapping using GIS and remote sensing databases for Al Baha Region Saudi Arabia, Appl. Sci. 12 (16) (2022) 8115, https://doi.org/10.3390/app12168115.
[72] M. Alsharif, A.A. Alzandi, R. Shrahily, B. Mobarak, Land use land cover change analysis for urban growth prediction using landsat satellite data and Markov chain model for Al Baha Region Saudi Arabia, Forests 13 (10) (2022) 1530, https://doi.org/10.3390/f13101530.
[73] S.H. Alsultan, A.A. Rahman, Kingdom of Saudi Arabia geospatial information infrastructure–an initial study, Int. Arch. Photogram. Rem. Sens. Spatial Inf. Sci. 40 (2015) 95, https://doi.org/10.5194/isprsarchives-XL-2-W4-95-2015.
[74] M. Van Den Eeckhaut, J. Poesen, G. Verstraeten, V. Vanacker, J. Moeyersons, J. Nyssen, L.P.H. Van Beek, The effectiveness of hillshade maps and expert knowledge in mapping old deep-seated landslides, Geomorphology 67 (3–4) (2005) 351–363.
[75] Y. Noh, S. Park, S.B. Park, Aspect-based sentiment analysis using aspect map, Appl. Sci. 9 (16) (2019) 3239, https://doi.org/10.3390/app9163239.
[76] J. De Reu, J. Bourgeois, M. Bats, A. Zwertvaegher, V. Gelorini, P. De Smedt, W. Chu, M. Antrop, P. De Maeyer, P. Finke, M. Van Meirvenne, J. Verniers, P. Crombé, Application of the topographic position index to heterogeneous landscapes, Geomorphology 186 (2013) 39–49, https://doi.org/10.1016/j.geomorph.2012.12.015.
[77] M. Różycka, P. Migoń, A. Michniewicz, Topographic wetness index and terrain ruggedness index in geomorphic characterisation of landslide terrains, on examples from the sudetes, SW Poland. Z, Geomorphology Suppl (2017) 61, https://doi.org/10.1127/zfg_suppl/2016/0328.
[78] P.A. Burrough, et, R.A. McDonell, Principles of Geographical Information Systems, Oxford University Press, New York, 1998, p. 190.
[79] H. Liu, R. Bu, J. Liu, W. Leng, Y. Hu, L. Yang, H. Liu, Predicting the wetland distributions under climate warming in the great xing'an mountains, northeastern China, Ecol. Res. 26 (3) (2011) 605–613, https://doi.org/10.1007/s11284-011-0819-2.
[80] D. Deumlich, R. Schmidt, M. Sommer, A multiscale soil–landform relationship in the glacial-drift area based on digital terrain analysis and soil attributes, J. Plant Nutr. Soil Sci. 173 (6) (2010) 843–851, https://doi.org/10.1002/jpln.200900094.
[81] B. Mobarak, R. Shrahily, A. Mohammad, A.A. Alzandi, Assessing green infrastructures using GIS and the multi-criteria decision-making method: the case of the al Baha region (Saudi Arabia), Forests 2022 13 (12) (2013), https://doi.org/10.3390/f13122013.
[82] A. Weiss, Topographic position and landforms analysis, in: Poster Presentation, ESRI user conference, San Diego, *CA*, 2001, p. 200.
[83] S.J. Riley, S.D. DeGloria, R. Elliot, A terrain ruggedness index that quantifies topographic heterogeneity, Intermt. J. Sci. 5 (1–4) (1999) 23–27.
[84] L.N. Kantakumar, P. Neelamsetti, Multi-temporal land use classification using hybrid approach, Egyp. J. Rem. Sens. Space Sci. 18 (2) (2015) 289–295, https://doi.org/10.1016/j.ejrs.2015.09.003.
[85] P. Verma, A. Raghubanshi, P.K. Srivastava, A.S. Raghubanshi, Appraisal of kappa-based metrics and disagreement indices of accuracy assessment for parametric and nonparametric techniques used in LULC classification and change detection, Model. Earth Sys. Environ. 6 (2) (2020) 1045–1059, https://doi.org/10.1007/s40808-020-00740-x.
[86] R. Manandhar, I.O.A. Odeh, T. Ancev, Improving the accuracy of land use and land cover classification of landsat data using post-classification enhancement, Rem. Sens. 1 (2009) 330–344, https://doi.org/10.3390/rs1030330.
[87] Saudi Arabia National Portal. Available at: https://www.my.gov.sa/wps/portal/snp/aboutksa/geospatialandgeographicinformation. Accessed in: 1/January/2023.
[88] Geospatial information is supportive and enabling to achieve the goals of the kingdom's vision 2030, Available at: https://gasgi.gov.sa/Ar/about/Pages/GeospatialInformationVision2030.aspx. (Accessed 21 January 2023).
[89] Register for National Geospatial Platform. Available at: https://geoportal.gasgi.gov.sa/RegApp/Account/Registration?returnUrl=https%3A%2F%2Fgeoportal.gasgi.gov.sa%2Fportal%2Fapps%2Fsites%2F%23%2Fgasgi-geoportal. Accessed in: 21/January/2023.
[90] Urban planning trends and challenges in the pursuit of Saudi vision 2030, Available at: http://www.ksclg.org/publication-project/english-urban-planning-trends-and-challenges-in-the-pursuit-of-saudi-vision-2030. (Accessed 21 January 2023).

[91] S.J. Khusaifan, The impact of the red Sea level rise on jeddah's coastal districts, western Saudi Arabia, JKAU: Met. Env. Arid Land Agric. Sci 29 (1) (2020) 59–77.
[92] M. El Raey, Impact of Sea Level Rise on the Arab Region, The University of Alexandria. *Arabian Academy of Science, Technology, and Maritime*, 2010.
[93] M.E. Hereher, Vulnerability assessment of the Saudi Arabian Red Sea coast to climate change, Environ. Earth Sci. 75 (2016) 30, https://doi.org/10.1007/s12665-015-4835-3.
[94] Y. Aina, K. Aleem, Assessing the vulnerability of an industrial city to predicted sea level rise using SRTM and GPS observations: the case of Yanbu, Saudi Arabia, Int. J. Geoinfor. 10 (3) (2014).
[95] J.A. Bahrawi, M. Elhag, Simulation of sea level rise and its impacts on the western coastal area of Saudi Arabia, Ind. J. Geo-Mar. Sci. 45 (1) (2016) 54–61.